RSC Advances

ROYAL SOCIETY OF CHEMISTRY

www.rsc.org/advances

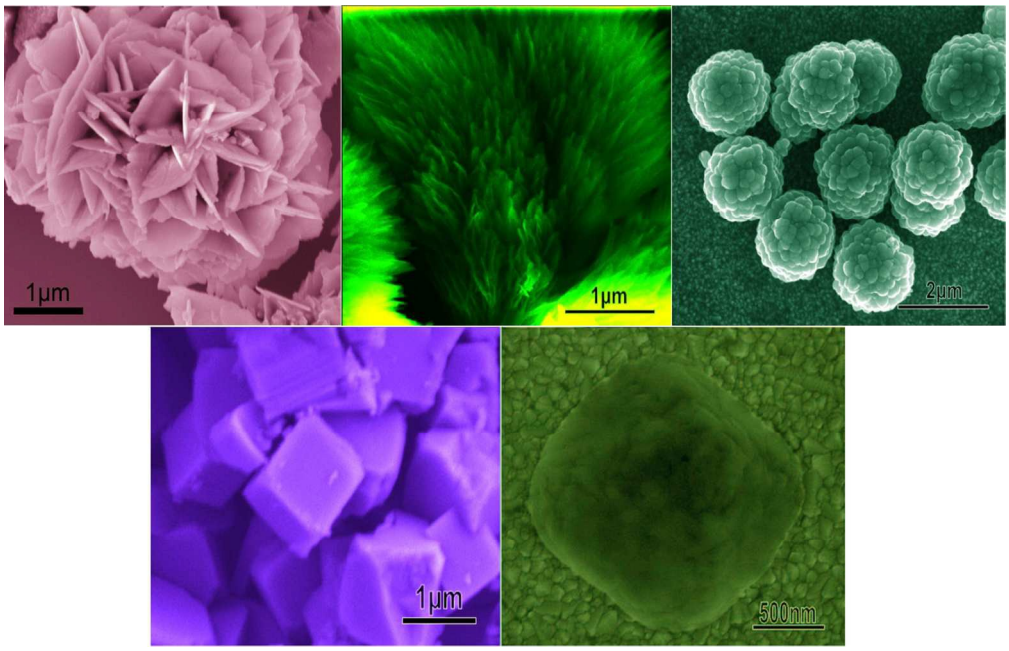

Nanostructured TiO2 particles with different morphologies obtained by a universal method.
120x76mm (300 x 300 DPI)

Abstract:
Nanostructured TiO_2 particles with various morphologies play an important role in photoelectricity and photocatalysis. In this work, we demonstrate how to tune the morphologies of TiO_2 particles. TiO_2 particles with well defined morphologies, for example, spherical flower, thatch, cauliflower, nanocube and octahedron were synthesized by a solvothermal route. This was realized by the effective control of the alcoholysis rate of TiF_4 and the prevention of the aggregation through optimizing the pressure, composition and pH value of the reaction solution. This work provides not only a strategy for controlling the morphology of TiO_2 particles, but also a universal method that can be applied to the preparation of other nanomaterials.

RSC Advances

Dynamic Article Links ►

Cite this: DOI: 10.1039/c0xx00000x

www.rsc.org/xxxxxx

PAPER

Morphology engineering of nanostructured TiO_2 particles

Ruhua Zha,[a] Reddeppa Nadimicherla,[a] Xin Guo*[a]

Received (in XXX, XXX) Xth XXXXXXXXX 20XX, Accepted Xth XXXXXXXXX 20XX
DOI: 10.1039/b000000x

Nanostructured TiO_2 particles with various morphologies play an important role in photoelectricity and photocatalysis. In this work, we demonstrate how to tune the morphologies of TiO_2 particles. TiO_2 particles with well defined morphologies, for example, spherical flower, thatch, cauliflower, nanocube and octahedron were synthesized by a solvothermal route. This was realized by the effective control of the alcoholysis rate of TiF_4 and the prevention of the aggregation through optimizing the pressure, composition and pH value of the reaction solution. This work provides not only a strategy for controlling the morphology of TiO_2 particles, but also a universal method that can be applied to the preparation of other nanomaterials.

Introduction

Nano titanium dioxide (TiO_2) is one of the most important nanostructured materials owing to their applications in water splitting,[1-3] dye-sensitized solar cells,[4] electrochromic devices[5] and photo degradation of organics.[6] Meanwhile, it is also one of the most promising semiconducting materials for photovoltaic, sensing applications due to its wide band gap, environmental friendliness and low cost.[7] Particularly, TiO_2 nanoparticles are the only substance in practical use today as a photocatalyst due to their various morphologies and high surface area.[8-10]

There is a strong relationship between the specific physical and chemical properties of nanostructured TiO_2 particles with its phase composition, specific surface area, pore size distribution, particle morphology and surface defects. It was reported that TiO_2 particles with porous morphologies had a significant impact on degradation and scavenging pollutants in water and air owing to their large surface area.[11] The spherical structures with a high surface area and narrow pore size distribution have great potential in solar energy conversion.[12] And well-defined anatase TiO_2 particles with exposed (001) crystal facets can enable a range of catalytic applications.[13] Hence, it is necessary to develop synthetic strategies, in which size and morphology of materials can be precisely controlled with designed functionalities.

Various techniques, e.g. sol-gel,[14] chemical vapour deposition (CVD),[15] microemulsion method[16] and pyrolysis,[17] etc, have been developed to synthesize nanostructured TiO_2 particles with defined structural architectures,[18] e.g. nanoparticles,[19,20] nanowires,[21] nanotubes,[22] single crystalline particles,[23-26] thin films[27,28] and nanosheets.[29-31] The sol-gel method is easy in operation, nevertheless, the TiO_2 nanostructure thus synthesized is always with smooth surfaces, lack of sharp edges, corners and which leads to lack of active sites for reaction on the surfaces.[32] With the CVD method, the morphology of the TiO_2 nanostructure is lack of variety. With the microemulsion method, the diameter of the dispersed droplets ranging from 5 to 100 nm is so small that the nucleation, particle growth, aggregation and particle agglomeration process are restricted.[16] With chemical precipitation method, the kinetics of the nucleation and particle growth in homogeneous solutions cannot be easily adjusted to produce monodisperse nanoparticles with narrow size distributions.[17] Therefore, the controllable synthesis of nanostructured TiO_2 with tuneable shapes and sizes is still a challenge and need thorough research.

Several phenomena, e.g. oriented attachment,[33-35] Ostwald ripening,[36] Kirkendall effect,[37] and the wet-etching,[38] are very helpful for the formation of complex nanostructures. Oriented aggregation is a special case of aggregation that provides an important route by which nanocrystals grow, defects are formed, and unique, often symmetry-defying, crystal morphologies are produced.[35] Mass transport via Ostwald ripening has been proven to be a facile approach to generate symmetric or asymmetric interior spaces, such as, core-shell structures.[39,40] In the Kirkendall effect, atomic diffusion occurs through vacancy exchange and not by the direct interchange of atoms, which directly leads to the formation of hollow nanocrystals.[41,42] The fluoride-mediated coordination-assisted etching can construct novel structures.[43]

In this work, we developed a solvothermal approach, with which we synthesized a series of nanostructured TiO_2 particles with various morphologies and well-tailored shapes and sizes, namely spherical flower, thatch, cauliflower, nanocube and octahedron. The synthetic method is versatile for the synthesis of different types of heterogeneous nanostructures, and it is a simple one-pot reaction, requires no complex devices. The morphology engineering of the nanostructured TiO_2 particles were achieved through selective etching to form different morphologies by controlling the quantity of etching agent, Ostwald-ripening and vertex-selective etching effect to finely control the sharp edges and corners in the surface of TiO_2 particles.

2. Experimental

2.1 Synthesis of nanostructured TiO_2 particles

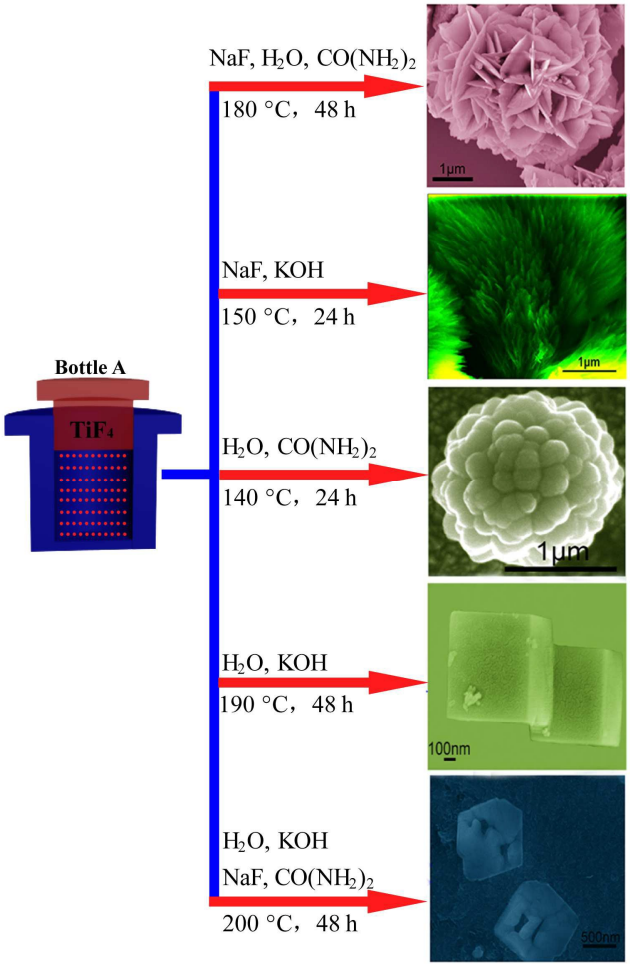

Fig. 1 Schematic illustration for the effects of different reagents on the final products.

The synthesis process is illustrated in Fig. 1. The titanium source of this work is TiF_4, and the TiF_4 solution (bottle A) was prepared by adding 0.3g TiF_4 (Alfa Aesar, 98%) into 61 ml absolute ethanol solution (Alfa Aesar, AR) during vigorous stirring for 60 minutes. The mixed solution (bottle B) consisted of various contents of etching agent (NaF), pH controlling agent (KOH) and slow-release basic reagent [$Co(NH_2)_2$]. Then these two solutions (bottle A and bottle B) were mixed under stirring, and it was transferred into a 100 ml autoclave and heated to a definite temperature for a certain time, then cooled to room temperature. The final products were centrifuged, and then rinsed with distilled water and ethanol several times to remove any fluoride remain in the final yield, finally dried at 80 °C for 24 h.

Spherical flower: 0.5 g NaF (Alfa Aesar, AR) and 2 g $CO(NH_2)_2$ (Alfa Aesar, AR) were dissolved in 14 ml distilled water to get the bottle B solution. The mixed solution of bottles A and B was then solvothermally treated in a 100 ml autoclave at 180 °C for 48 h.

Thatch: 1 g NaF and 0.1 g KOH (Alfa Aesar, AR) were dissolved in 14 ml ethanol to get the bottle B solution. The mixed solution of bottles A and B was then solvothermally treated in a 100 ml autoclave at 150 °C for 24 h.

Cauliflower: 1 g $CO(NH_2)_2$ was dissolved in 10 ml distilled water to get the bottle B solution. The mixed solution of bottles A and B was then solvothermally treated in a 100 ml autoclave at 140 °C for 24 h.

Nanocube: 0.5 g KOH was dissolved in 25 ml distilled water to get the bottle B solution. The mixed solution of bottles A and B was then solvothermally treated in a 100 ml autoclave at 190 °C for up to 48 h.

Octahedron: 0.5 g NaF, 0.6 g KOH and 0.69 g $CO(NH_2)_2$ were dissolved in 20 ml distilled water to get the bottle B solution. The mixed solution of bottles A and B was then solvothermally treated in a 100 ml autoclave at 200 °C for up to 48 h.

2.2 Characterization

Powder X-ray diffraction (XRD) spectra were carried out using a Philips diffractometer (PW 3050) operated at 40 kV and 40 mA with Cu-Kα monochromatic radiation, at the Bragg's angle range from 20° to 80°. The chemical characteristics of the adsorbents were analyzed by a Bruker VERTEX 70 Fourier transform infrared spectrometer (FT-IR). Raman spectra of the samples were collected at room temperature by a micro-Raman spectroscopy (HR-800 LabRaman, Jobin Yvon, Longjumeau, France). The system included an integral Raman microscope, a stigmatic single spectrograph and a Peltier-cooled charge coupled device detector. The microscope attachment was an Olympus BX41 system and using excitation with 10 mW Ar^+ laser light (k = 514.532 nm). The spectral resolution was about 1–2 cm^{-1}. X-ray Photoelectron Spectroscopy (XPS) measurements were conducted using a VG MultiLab 2000 system with a monochromatic Al Ka X-ray source (ThermoVG Scientific). The binding energy was calibrated with the C 1s signal at 284.5 eV. The spherical flowers, thatches, cauliflowers, nanocubes and octahedra were characterized by scanning electron microscopy (SEM, Nova NanoSEM450). Transmission electron microscopy (TEM) observation was carried out using a JEOL 2100F microscopy. And the surface area was calculated using a multipoint Brunauer-Emmett-Teller (BET) model by nitrogen physisorption at -196 °C with a Micrometritics ASAP 2020 analyzer. The pore size distribution (PSD) was obtained via a non-local density functional theory (NLDFT) method by using nitrogen adsorption data and assuming a slit pore model.[44,45]

3. Results and Discussion

3.1. Structure

The XRD patterns of spherical flowers, thatches, cauliflowers, nanocubes and octahedra are plotted in Fig. 2. These samples exhibit diffraction peaks at (101), (103), (004), (200), (105), (211), (204), (116), (220) and (215) planes for the anatase structure, demonstrating that the synthesized TiO_2 particles are well-crystallized in the anatase phase. The absence of diffraction peaks at 27° and 31° demonstrates that the TiO_2 samples are free of rutile and brookite structures.

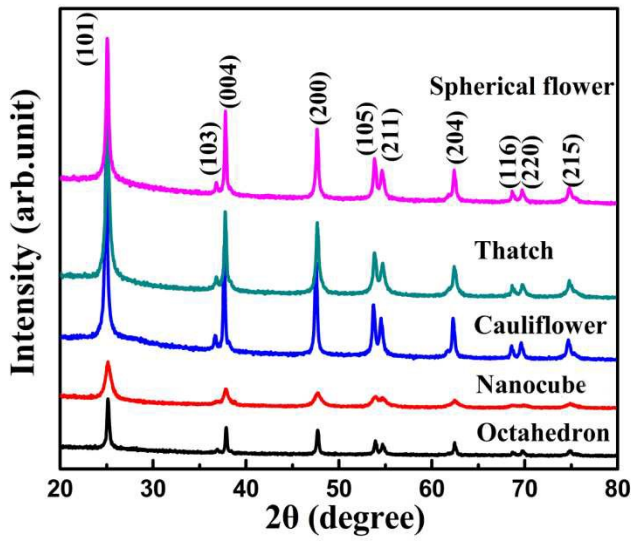

Fig. 2 XRD patterns of TiO_2 spherical flowers, thatches, cauliflowers, nanocubes, octahedra.

The Raman spectra of TiO_2 spherical flowers, thatches, cauliflowers, nanocubes and octahedra are given in Fig. 3. Strong bands are observed at 145, 200, 402, 522 and 642 cm^{-1}, corresponding to the anatase phase. All these characteristic bands are due to the five Raman-active modes of anatase phase with the symmetries of E_g, E_g, B_{1g}, B_{1g} and E_g,[46] respectively. The band at 447 cm^{-1}, which is due to E_g modes of rutile phase,[47] could not be observed explicitly. Obviously, the Raman results agree with the XRD analysis very well.

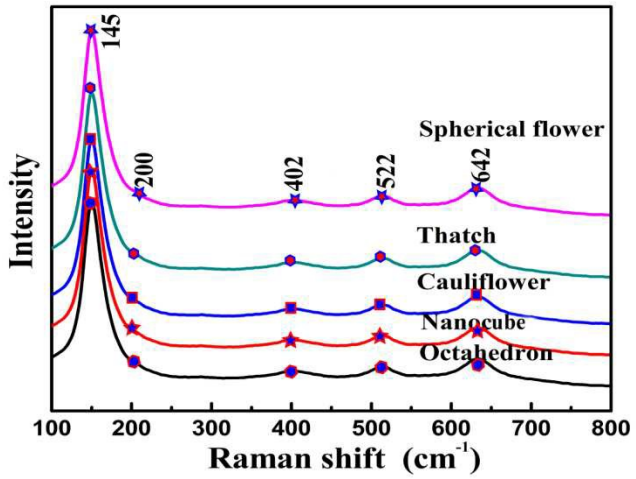

Fig. 3 Raman spectra of TiO_2 spherical flowers, thatches, cauliflowers, nanocubes, octahedra.

3.2. Morphology

Spherical flower:

Fig. 4 shows the morphological evolution of spherical flowers at different stages of the solvothermal treatment. After 1 h solvothermal reaction at 180 °C (Fig. 4A), a large number of nanoparticles with a diameter of about 11 nm were produced. When the reaction time was 4 h (Fig. 4B), some partially formed embryos of microspheres could be observed. The irregular embryonic microspheres were stacked together. When the reaction time was prolonged to 48 h, microspheres with well-developed morphology could be seen (Fig. 4C). During the solvothermal reaction, the diameter of the microspheres hardly changed, but the nanosheets grew larger and gradually showed clear edges. The morphology can be clearly observed in Figs. 4D and E; the spherical flowers consist of multi-layer nanosheets. The nanosheets are single crystalline, and the obvious lattice fringes shown in Fig. 4F can be assigned to the *d* spacing value of (101) plane in the anatase structure.

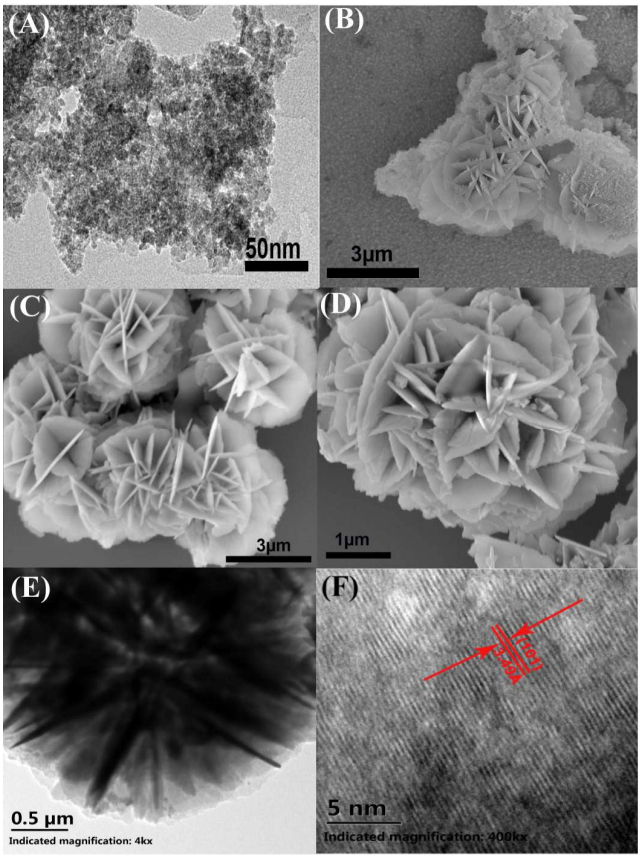

Fig. 4 Evolution of spherical flowers at different stages: (A) 1 h, (B) 4 h, (C) 48 h, (D) magnified SEM image, (E) TEM image and (F) high resolution TEM image of TiO_2 spherical flowers.

The occurrence of the intermediates suggests that there are two growth stages; one refers to the nucleation and growth of the nanosheets, and the other refers to the formation of the rose-like nanostructures. On the basis of the above XRD analysis, SEM and TEM observations, the formation mechanism of TiO_2 hierarchical microspheres can be rationalized by an aggregation and dissolution-recrystallization process (Fig. 5). At the beginning of the reaction, large amount of nanoparticles were produced by alcoholysis of TiF_4 due to relatively high temperature (180 °C) and pH value. The appropriate pH value was maintained by $CO(NH_2)_2$. Then these nanoparticles aggregated into nanosheets to reduce the surface energy. The spontaneous growth of the nanosheets was generated by a dissolution-recrystallization process followed by the Ostwald ripening. It was the etching of the high concentration of F^- (NaF) that made the aggregated nanosheets become thinner in the process of the Ostwald ripening.[48,49] With the reaction time extending, the spherical flower structure was formed with a bunch of nanosheets standing on the surfaces.

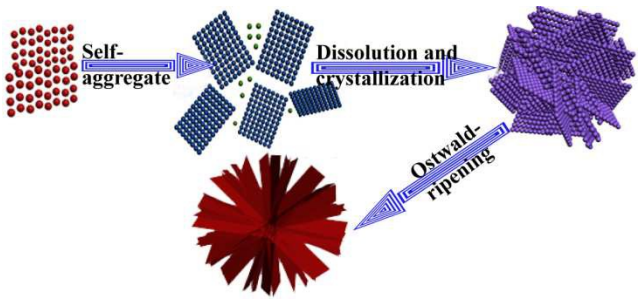

Fig. 5 Schematic illustration of the formation of spherical flower.

Thatch:

The time dependent morphology evolution of thatches is shown in Fig. 6. The solvothermal reaction was carried out at a relatively low temperature of 150 °C. After a short time of 1.5 h, TiO_2 microspheres with an average diameter of ca. 1.5-2 μm were formed (Fig. 6A). As the time increased to 24 h, thatches (Figs. 6B and C) were produced, consisting of numerous nanowires. According to the TEM image in Fig. 6D, these nanowires have uniform diameters of ~6 nm.

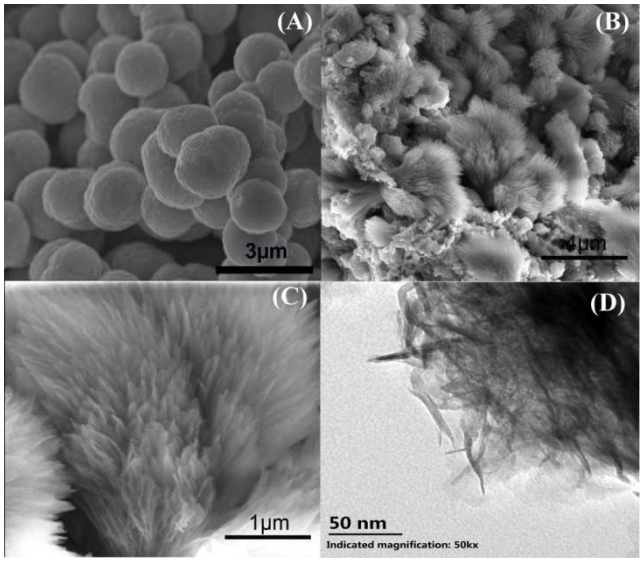

Fig. 6 Evolution of thatches at different stages: (A) 1.5 h, (B) 24 h, (C) magnified SEM image and (D) TEM image of TiO_2 thatches.

Fig. 7 depicts the possible formation mechanism of thatches. In the alkali solution of KOH and at 150 °C, initially nanoclusters are formed and spontaneously aggregate to large particles to minimize the surface area. As a kinetically controlled process, the crystal growth is initiated preferentially from the active clusters on the surfaces of the particles, owing to the high concentration of F^-. The subsequent growth along the c axis produces the morphology of thatch.

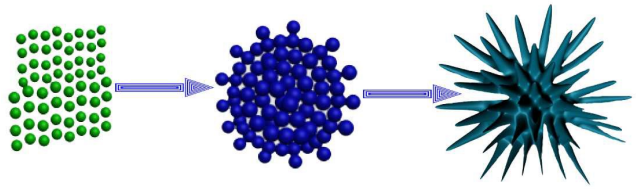

Fig. 7 Schematic illustration of the formation of thatch.

Cauliflower:

The morphology evolution of cauliflowers is shown in Fig. 8. Initially TiO_2 microspheres with an average diameter of ca. 1-1.5 μm were formed after 2 h of solvothermal reaction, and cauliflowers with well-developed morphology were formed after 24 h (Fig. 8B). The cauliflowers are composed of many ordered small balls.

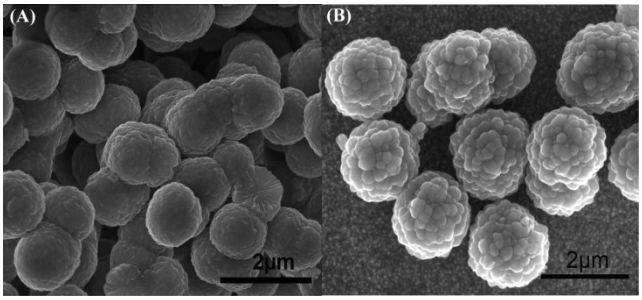

Fig. 8 Evolution of cauliflowers at different stages: (A) 2 h and (B) 24 h.

Plausible formation mechanism of the cauliflowers is illustrated in Fig. 9. We propose that the cauliflowers are formed by a two-step process, i.e., an aggregation process and oriented attachment. In the first step, nanoparticles are generated by the alcoholysis of TiF_4, followed by aggregation into small balls. The formation of TiO_2 small balls is due to the rational pH value and pressure. In the synthesis of the cauliflowers, $CO(NH_2)_2$ is added as a slow-release basic reagent to adjust the pH value of the reaction solution, and the pressure is controlled by the appropriate temperature of 140 °C. In the second step, the cauliflowers are formed by the oriented attachment of TiO_2 small balls.

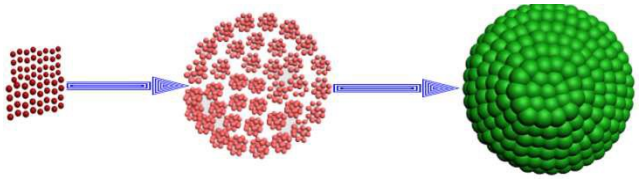

Fig. 9 Schematic illustration for the two-step changes involved in the formation of cauliflower structure.

Nanocube:

Fig. 10 shows the evolution of nanocubes. Initially TiO_2 nanoparticles were obtained. As the time increased to 8 h, these nanoparticles spontaneously aggregated to large particles (Fig. 10A). Then these particles were transformed into cubes when the reaction time increased to 48 h (Fig. 10B).

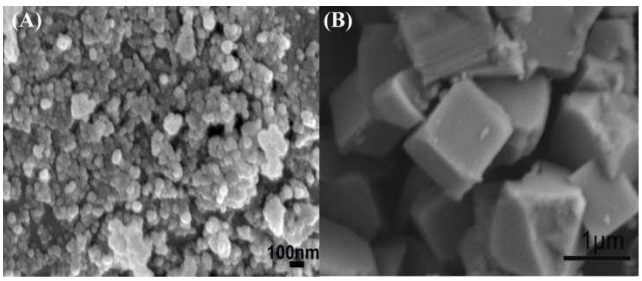

Fig. 10 Evolution of nanocubes at different stages: (A) 8 h and (B) 48 h.

Fig. 11 shows the possible formation mechanism of the nanocubes. In the reaction system accelerated by the alkali solution of KOH, TiF_4 is alcoholized at 190 °C to form numerous

nanoparticles, and the nanoparticles spontaneously aggregated to large particles to minimize the surface area. Then the cube-like architectures are formed by the oriented attachment of scattered nanoparticles. Finally, small cubes are gradually transformed into compact and bigger cubes.

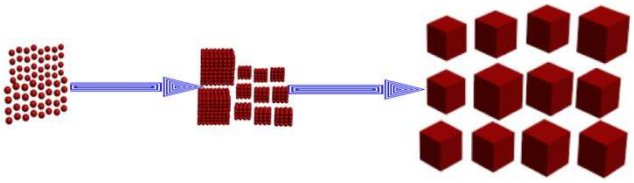

Fig. 11 Schematic illustration for the formation of TiO_2 nanocubes.

Octahedron:

The morphology evolution of the octahedra is shown in Fig. 12. After alcoholysis for 1 h, quasi-octahedral particles with rugged surfaces were obtained (Fig. 12A). The inset in Fig. 12A shows a single octahedron with ~900 nm edges. When the reaction time was increased to 5 h, octahedral crystals with holes on the apexes as well as pores in the interiors were observed (Fig. 12B). Octahedral cages were formed by the gradual etching from the surface into the interior after an aging for 48 h (Fig. 12C). Fig. 12D presents the magnified SEM image of two octahedral cages. The hollow octahedra were gradually etched into fragments when the aging time was further increased.

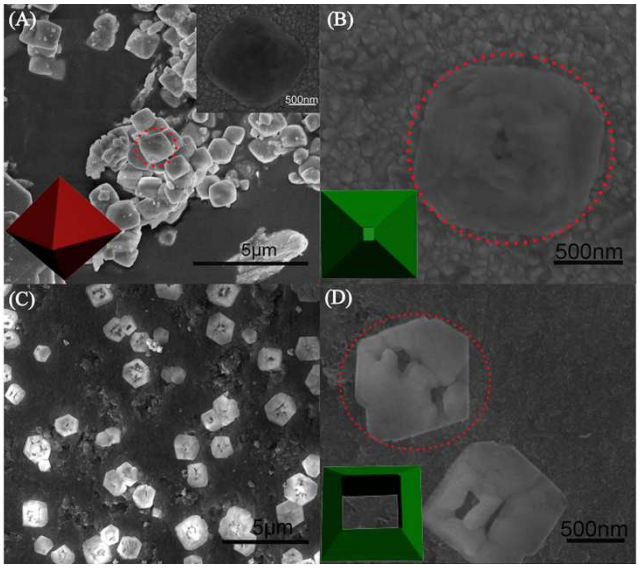

Fig. 12 Evolution of octahedra at different stages: (A) 1 h, (B) 5 h, (C) 48 h, and (D) magnified SEM image of octahedral cages.

The octahedra are probably formed by a three-step process, i.e., the self-aggregation of nanoparticles, Ostwald-ripening and vertex-selective etching, as illustrated in Fig. 13. Firstly, the octahedra are formed via the oriented attachment of nanoparticles, and then the octahedra are gradually transformed from non-compact architecture into hollow octahedra, in which the formation of partially hollow octahedra stems from an evacuation process from the apexes. The formation of octahedra relies on appropriate pH value and pressure; the pH value is maintained by the proper combination of $CO(NH_2)_2$ and KOH, and the pressure is controlled by temperature (200 °C). Lastly, F^- assisted vertex-selective etching leads to the evacuation of the cages' eight surfaces and the formation of the frames.

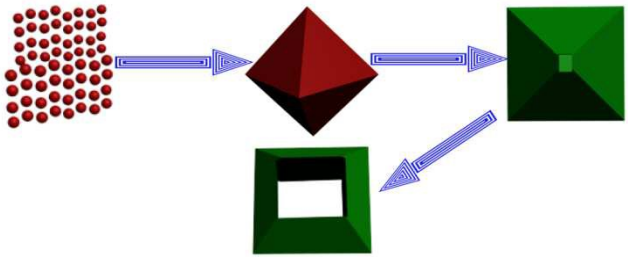

Fig. 13 Schematic illustration for the three-step formation process of TiO_2 octahedron.

The formation mechanism described in this work offers several instructions. Generally, the nanostructured TiO_2 particles are formed by the processes of aggregation, Ostwald ripening and etching. Firstly, TiO_2 nanoparticles are produced by the alcoholysis of TiF_4 at temperatures above 140 °C. Then these nanoparticles are quickly aggregated into various intermedia, such as nanosheets, small balls, and hollow octahedra, etc. Afterwards, the TiO_2 intermedia spontaneously generate a dissolution-recrystallization process by the Ostwald ripening. At last, the final morphologies are formed by the F^- assisted vertex-selective etching. The factors determining the formation of spherical flowers, thatches, cauliflowers, nanocubes and octahedra are temperature, pH value and composition of the solvothermal reaction. The temperature of the solvothermal reaction is crucial to the aggregation of the TiO_2 nanoparticles obtained in the initial stage of reaction. The pH value of the reaction solution plays an important role in determining the Ostwald ripening. The keen smooth surface is observed at higher pH value (controlled by the amount of KOH, ammonia or urea), which is evidenced from the comparison of nanocubes, octahedra. The etching agent of NaF can provide assisted selective etching for the final morphologies.

3.3. BET

To understand the special morphologies of the nanostructured TiO_2 particles, nitrogen adsorption–desorption isotherms and corresponding pore size distributions were investigated, and the results are shown in Fig. 14. The nanocubes and octahedra (Figs. 14A, B) can be characterized as type III features. The isotherms illustrate a weak adsorption interaction between nitrogen and the TiO_2 particles, suggesting that no micropores or mesopores exist in the TiO_2 particles. However, there is a sharp increase with adsorption volume in the relative pressure range of 0.86–0.99, indicating the presence of macropores. This may be due to the existence of the hollow structure or interparticulate space. The cauliflowers, thatches and spherical flowers (Figs. 14C, D) can be characterized by the reversible type II isotherm, which is a normal form of isotherm obtained with a non-porous or macroporous adsorbent. The type II isotherm represents unrestricted monolayer-multilayer adsorption. The surface area, pore volume and average pore size calibrated from Fig. 14 are given in Table 1.

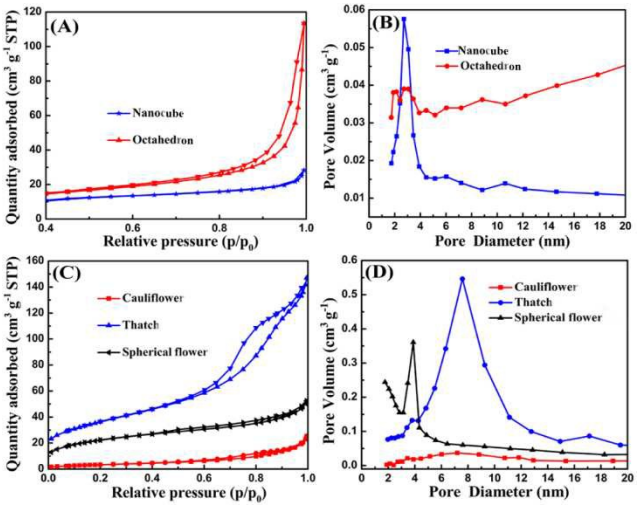

Fig. 14 (A and C) Nitrogen adsorption–desorption isotherms, and (B and D) corresponding pore size distributions of the nanostructured TiO_2 particles.

3.4. Valence state

To get an in depth understanding of the composition and chemical state of the nanostructured TiO_2 particles, the samples were investigated by XPS, and the spectra for the TiO_2 thatches are given in Fig. 15. Fig. 15A shows the survey wide-scan spectrum for the TiO_2 thatches. Narrow scan multiplex spectra were obtained for O 1s and Ti 2P elements and the Ti LMM and O KLL Auger peaks were also obtained at binding energies of 1105 and 976 eV, respectively. The Ti 2p core level spectrum is shown in Fig. 15B. The Ti 2p curve consists of two distinct Ti 2p3/2 and Ti 2p1/2 photopeaks with the binding energies of 458.8 and 464.4 eV, respectively. It can be seen that two peaks are highly symmetrical and no shoulders are observed, indicating that the formation of stoichiometric TiO_2. The peaks are not very broad and no shoulder peaks are observed, which are identical with those reported by Siemensmeyer and Schultze.[50] The energy value observed at 458.8 eV indicates the presence of Ti^{4+}. The spectrum of O 1s composed of two peaks is shown in Fig. 15C. The first strong peak observed at a binding energy of 529.8 eV is related to bulk oxygen bonding with titanium (Ti-O), while the second one at 531.6 eV corresponds to the hydroxyl group (Ti-OH), which are consistent with the FT-IR analysis.[51,52] The XPS results demonstrate the existence of Ti–OH groups.

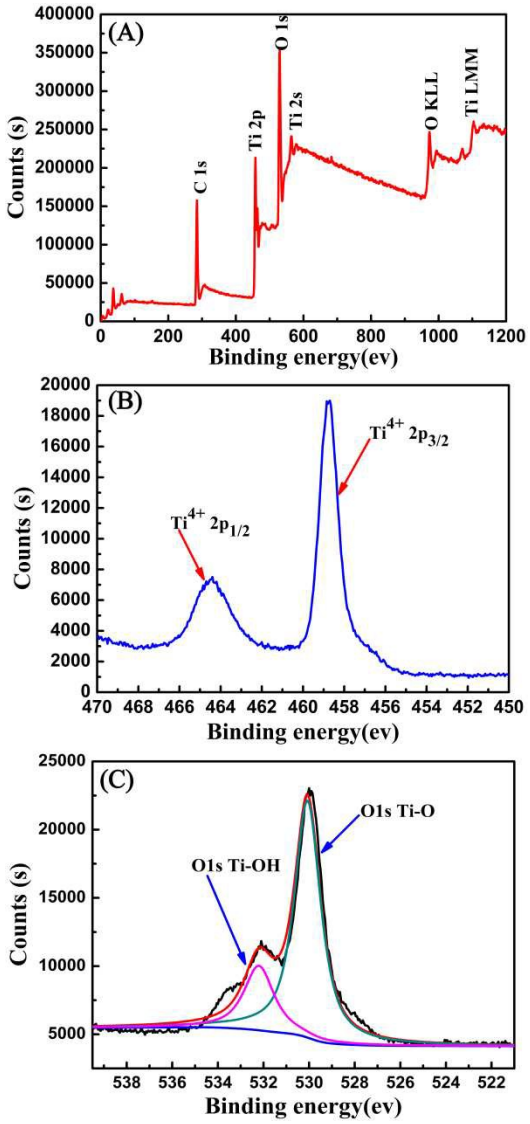

Fig. 15 XPS spectra of thatches: (A) wide-survey spectrum, (B) Ti 2p core level and (C) O 1s core level.

The FT-IR spectra of the spherical flowers, thatches, cauliflowers, nanocubes and octahedra are shown in Fig. 16. The FT-IR spectra are almost the same for the different samples. The broad peaks observed at 3434.8 cm^{-1} correspond to the stretching vibration of surface hydroxyls and adsorbed water.[53] The peaks at 1635.9 cm^{-1} are due to the bending vibration of Ti-OH. The bands at about 1401.9 cm^{-1} are related to the bending vibration of Ti-O-Ti. And the bands at below 800 cm^{-1} are due to the Ti-O stretching vibration. These results are consistent with those reported by Shabalin.[54,55]

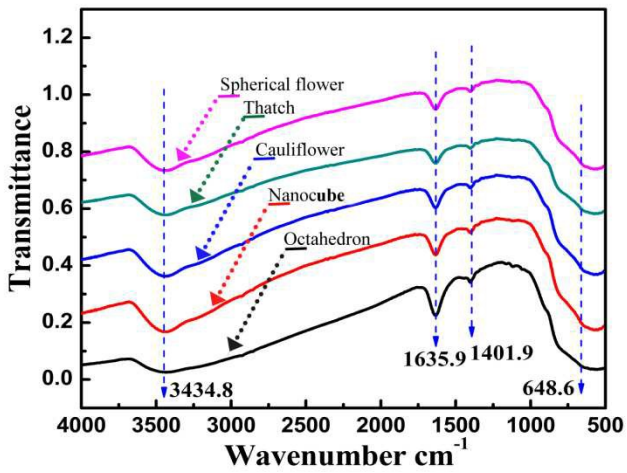

Fig. 16 FT-IR spectra of TiO_2 spherical flowers, thatches, cauliflowers, nanocubes, octahedra.

Table 1 Properties of TiO_2 particles with various morphologies

Sample	BET surface area ($m^2 g^{-1}$)	Pore volume ($cm^3 g^{-1}$)	Average pore size (nm)
Spherical flower	172.02	0.1224	4.5
Thatch	127.99	0.2233	7.13
Cauliflower	12.86	0.0379	11.06
Nanocube	28.47	0.2342	6.22
Octahedron	41.26	0.1711	16.68

4. Conclusions

A systematic approach was applied to solvothermally synthesize nanostructured TiO_2 particles with five types of morphologies, namely spherical flower, thatch, cauliflower, nanocube, octahedron. These nanostructured particles are stoichiometric, crystallized with the anatase structure, the BET surface areas vary for more than one order of magnitude from 12.86 to 172.02 m^2g^{-1}, and pore size from 3.96 to 16.68 nm. The synthesis of nanostructured TiO_2 particles with tuneable shapes and sizes were achieved through controlling the alcoholysis rate of TiF_4, the aggregation of morphology control agent, pressure, and pH value of the reaction solution. This work provides not only a strategy for controlling the size and morphology of TiO_2 particles, but also a facile and universal method that can be applied to the preparation of other nanostructured materials.

Notes and references

[a] *Laboratory of Solid State Ionics, School of Materials Science and Engineering, Huazhong University of Science and Technology, Wuhan 430074, P.R. China*
** Author to whom correspondence should be addressed.*
Tel: +86-27-87559804; Fax: +86-27-87559804; E-mail: xguo@hust.edu.cn

1 F. E. Osterloh, *Chem. Mater.*, 2007, **20**, 35.
2 S. U. M. Khan, M. Al-Shahry and W. B. Ingler, *Science*, 2002, **297**, 2243.
3 G. K. Mor, K. Shankar, M. Paulose, O. K. Varghese and C. A. Grimes, *Nano Lett.*, 2005, **5**, 191.
4 G. K. Mor, K. Shankar, M. Paulose, O. K. Varghese and C. A. Grimes, *Nano Lett.*, 2006, **6**, 215.
5 R. Cinnsealach, G. Boschloo, S. N. Rao and D. Fitzmaurice, *Sol. Energy Mater. Sol. Cells.*, 1999, **57**, 107.
6 X. B. Chen, L. Liu, P. Y. Yu and S. S. Mao, *Science*, 2011, **331,** 746.
7 X. Chen and S. S. Mao, *Chem. Rev.*, 2007, **107**, 2891.
8 B. O'Regan and M. Gratzel, *Nature*, 1991, **353**, 737.
9 T. Nonoyama, T. Kinoshita, M. Higuchi, K. Nagata, M. Tanaka, K. Sato and K. Kato, *J. Am. Chem. Soc.*, 2012, **134**, 8841.
10 J. C. Yu, L. Z. Zhang, Z. Zheng and J. C. Zhao, *Chem. Mater.*, 2003, **15**, 2280.
11 M. M. Khin, A. S. Nair, V. J. Babu, R. Murugan and S. Ramakrishna, *Energy Environ. Sci.*, 2012, **5**, 8075.
12 M. Pal, J. García Serrano, P. Santiago and U. Pal, *J. Phys. Chem. C.*, 2007, **111**, 96.
13 Y. Q. Dai, C. M. Cobley, J. Zeng, Y. M. Sun and Y. N. Xia, *Nano Lett.*, 2009, **9**, 2455.
14 L. L. Hench and J. K. West, *Chem. Rev.*, 1990, **90**, 33.
15 S. J. Song, Y. J. Park, J. Park, M. D. Cho, J. H. Kim, M. H. Jeong, Y. S. Kim and D. L. Cho, *J. Mater. Chem.*, 2010, **20**, 4792.
16 M. Andersson, L. Österlund, S. Ljungstroem and A. Palmqvist, *J. Phys. Chem. B.*, 2002, **106**, 10674.
17 C. Burda, X. B. Chen, R. Narayanan and M. A. EL-Sayed, *Chem. Rev.*, 2005, **105**, 1025.
18 D. Chen, L. Cao, F. Huang, P. Imperia, Y. B. Cheng and R. A. Caruso, *J. Am. Chem. Soc.*, 2010, **132**, 4438.
19 D. Li, H. Zhou and I. Honma, *Nat. Mater.*, 2004, **3**, 65.
20 Z. Q. Sun, J. H. Kim, Y. Zhao, F. Bijarbooneh, V. Malgras, Y. M. Lee, Y. M. Kang and S. X. Dou, *J. Am. Chem. Soc.*, 2011, **133**, 19314.
21 Z. Miao, D. S. Xu, J. H. Ouyang, G. L. Guo, X. S. Zhao and Y. Q. Tang, *Nano Lett.*, 2002, **2**, 717.
22 K. Shankar, J. I. Basham, N. K. Allam, O. K. Varghese, G. K. Mor, X. J. Feng, M. Paulose, J. A. Seabold, K. S. Choi and C. A. Grimes, *J. Phys. Chem. C.*, 2009, **113**, 6327.
23 H. G. Yang, C. H. Sun, S. Z. Qiao, J. Zou, G. Liu, S. C. Smith, H. M. Cheng and G. Q. Lu, *Nature*, 2008, **453**, 638.
24 F. Amano, O. Prieto-Mahaney, Y. Terada, T. Yasumoto, T. Shibayama and B. Ohtani, *Chem. Mater.*, 2009, **21**, 2601.
25 D. Q. Zhang, G. S. Li, X. F. Yang and J. C. Yu, *Chem. Commun.*, 2009, 4381.
26 H. G. Yang, C. H. Sun, S. Z. Qiao, J. Zou, G. Liu, S. C. Smith, H. M. Cheng and G. Q. Lu. *Nature*, 2008, **453**, 638.
27 S. Y. Choi, M. Mamak, N. Coombs, N. Chopra and G. A. Ozin, *Adv. Funct. Mater.*, 2004, **14**, 335.
28 E. L. Crepaldi, G. J. D. A. Soler-Illia, D. Grosso, F. Cagnol, F. Ribot and C. Sanchez, *J. Am. Chem. Soc.*, 2003, **125**, 9770.
29 X. G. Han, Q. Kuang, M. S. Jin, Z. X. Xie and L. S. Zheng, *J. Am. Chem. Soc.*, 2009, **131**, 3152.
30 G. Liu, H. G. Yang, X. W. Wang, L. N. Cheng, J. Pan, G. Q. M. Lu and H. Cheng, *J. Am. Chem. Soc.*, 2009, **131**, 12868.
31 H. G. Yang, G. Liu, S. Z. Qiao, C. H. Sun, Y. G. Jin, S. C. Smith, J. Zou, H. M. Cheng and G. Q. M. Lu, *J. Am. Chem. Soc.*, 2009, **131**, 4078.
32 Y. Wan and D. Y. Zhao, *Chem. Rev.*, 2007, **107**, 2821.
33 R. L. Penn and J. F. Banfield, *Am. Mineral.*, 1998, **83**, 1077.
34 R. L. Penn and J. F. Banfield, *Science*, 1998, **281**, 969.
35 R. L. Penn, *J. Phys. Chem. B.*, 2004, **108**, 12707.
36 W. Z. Ostwald, *Phys. Chem.*, 1900, **34**, 495.
37 E. O. Kirkendall, L. Thomassen and C. Upthegrove, *Trans. AIME.*, 1939, **133**, 186.
38 M. S. Minsky, M. White and E. L. Hu. *Appl. Phys. Lett.*, 1996, **68**, 1531.

39 B. Liu and H. C. Zeng, *Small*, 2005, **1**, 566.

40 J. J. Xie, Z. Y. Fu, Y. C. Wang, S. W. Lee and K. Niihara. *J. Am. Ceram. Soc.*, 2014, **34**, 13.e1.

41 Y. D. Yin, R. M. Rioux, C. K. Erdonmez, S. Hughes, G. A. Somorjai and A. P. Alivisatos, *Science*, 2004, 304, 711.

42 V. Kumari, A. K Patra and A. Bhaumik, *RSC Adv.,* 2014, 4, 13626.

43 J. Y. Zheng, X. Wang, W. Li, Z. W. Cao, H. Wang, C. Zhang, W. G. Song, Y. Ma and J. N. Yao, *CrystEngComm*, 2012, **14**, 7616.

44 M. Sevilla and A. B. Fuertes, *Energy Environ. Sci.*, 2011, **4**, 1765.

45 A. Shabaev and A. L. Efros, *Nano Lett.*, 2004, **4**, 1821.

46 J. Zhang, M. J. Li, Z. C. Feng, J. Chen and C. Li, *J. Phys. Chem. B.*, 2006, **110**, 927.

47 M. H. Ryu, K. N. Jung, K. H. Shin, K. S. Han and S. Yoon, *J. Phys. Chem. C.*, 2013, **117**, 8092.

48 P. Madhusudan, J. Zhang, B. Cheng and G. Liu, *CrystEngComm*, 2013, **15**, 231-240.

49 X. Wang, H. Fu, A. Peng, T. Zhai, Y. Ma, F. Yuan and J. Yao, *Adv. Mater*., 2009, **21**, 1636-1640.

50 B. Siemensmeyer and J. W. Schultze, *Surf. Interface Anal.*, 1990, **16**, 309.

51 R. H. Zha, R. Nadimicherla and X. Guo, *J. Mater. Chem. A*, 2014, **2**, 13932.

52 T. Prakash, M. Navaneethan, J. Archana, S. Ponnusamy, C. Muthamizhchelvan and Y. Hayakawa, *Mater. Res. Bull.*, 2013, **48**, 1541.

53 Z. Y. Liu, D. D. Sun, P. Guo and J. O. Leckie, *Chem. Eur. J*., 2007, **13**, 1851-1855.

54 S. Musić, M. Gotić, M. Ivanda, S. Popović, A. Turković, R. Trojko, A. Sekulić and K. Furić, *Mater. Sci. Eng. B*, 1997, **47**, 33-40.

55 S. F. Wang, F. Gu, M. K. Lü, C. F. Song, S. W. Liu, D. Xu and D. R. Yuan, *Mater. Res. Bull.*, 2003, **38**, 1283-1288.